Starch-based mechanically tough hydrogel for effective removal of toxic metal ions

Highlights

The current chapter describes the fabrication of mechanically tough hydrogel using a double cross-linking strategy. The first network of the hydrogel was prepared by starch cross-linked with epichlorohydrin, while acrylic acid cross-linked with *N, N*-methylene bisacrylamide was acted as the second network. The hydrogel was characterized by using different spectroscopic and analytical techniques. The highest mechanical strength was found to be 2.78±0.58 MPa for the synthesized hydrogel. More impressively, the hydrogel also exhibited excellent adsorption capacity for toxic metal ions for wastewater treatement. Additionally, the hydrogel showed outstanding reusability due to its excellent mechanical strength. Hence, the hydrogel can be utilized for the subsequent purification cycles. Thus, the synthesized material is promising as proficient toxic heavy metal ions adsorbent, as it meets the demand for soft matter with remarkable mechanical properties to satisfy recyclability.

Parts of this chapter are published as-

[1] Sarmah, D. and Karak, N. Starch based mechanically tough hydrogel for effective removal of toxic metal ions from wastewater. *Journal of Cleaner Production*, 344:131074, 2022.

4.1. Introduction

The previous chapter (**Chapter 3**) explored the fabrication of starch-based hydrogel with amphoteric properties. Although, the double network (DN) hydrogel was effective for the removal of both cationic and anionic dyes, but the preparative route was unable to provide a mechanically tough hydrogel. For the effective removal of pollutants from an aqueous medium, enough mechanical strength is of utmost importance for easy recoverability and recyclability [1]. But most of the conventional hydrogels were mechanically weak due to their irregular cross-linking pattern and as well as wide distribution of molecular chain length [2,3]. The brittleness character of these mechanically weak hydrogels causes secondary water pollution during adsorption and also low reusability [4]. Although literature advocates the utilization of enormous efforts for the development of mechanically tough hydrogel there are still lack of desirable strength. For example, Gong et al. prepared a poly(vinyl alcohol) and poly(acrylamide-co-acrylic acid (AA)) based self-healing hydrogel with the mechanical strength of 1.23± 0.09 MPa [3]. Yang et al. prepared an alginate/poly(acrylamide) based hydrogel using various multivalent cations with a maximum strength of 0.9391±0.0476 MPa [5]. These results show that the mechanical strength of these hydrogels was not up to the mark. However, Lin et al. prepared a poly(acrylamide-co-AA) based dual cross-linked hydrogel with the mechanical strength of 6 MPa [6], but use of only synthetic monomers restrict its application. At this end, development of a bio-based hydrogel with high toughness remains a daunting challenge. Therefore, in this work, we aimed to synthesize a starch-based double cross-linked hydrogel with enough mechanical strength by modifying the preparative method of the amphoteric hydrogel described in **Chapter 3**. To obtain the desired mechanical strength, starch was allowed to react with only epichlorohydrin (ECH) instead of the incorporation of triethylamine (TEA) groups [7]. The second network was formed by grafting poly(acrylic acid) (PAA) cross-linked by *N, N*-methylene bisacrylamide (MBA) onto the ECH cross-linked starch network. The elimination of TEA groups not only wiped out the amphoteric properties but also allowed the complete cross-linking of ECH with the hydroxyl groups of starch. Thus, the ECH cross-linking network improved the strength of the hydrogel and both the networks together result in a ductile and tough hydrogel, which further help for achieving deformation resistance and attaining high mechanical strength. Moreover, the carboxylate groups of PAA form electrostatic interaction with the metal ions present in

water and hence the hydrogel can be effectively used for metal ion-contaminated water purification. Inappropriate discharge of toxic metal ions from various industries such as smelting, mining, electronics, and battery manufacturing processes have notorious effects on water resources, and pullulated water has harmful effects on both aquatic life and other biological systems [8-10]. The removal of these hazardous pollutants from wastewater is of utmost importance and the synthesized hydrogel can be effectively used for metal ions adsorption with high recyclability. Our attempts promisingly shaped a facile approach to fabricate a starch-based hydrogel with favorable mechanical properties, which undoubtedly has potential application performance in sustainable environmental protection.

4.2. Experimental

4.2.1. Materials

Various chemicals including tapioca starch, AA, ammonium persulfate (APS), MBA, sodium hydroxide (NaOH), ECH, and hydrochloric acid (HCl) were used as the same grade and specifications as described in **Chapter 2** and **Chapter 3.**

Copper (II) chloride dihydrate is a blue-green color complex of copper with molecular weight 170.48 g/mol. It was received from Merck, India and the aqueous solution of it was used for the metal ions adsorption study.

Nickel (II) chloride hexahydrate was purchased from Merck, India. Its molecular weight is 237.69 g/mol and green in color. It was used for metal ion adsorption studies from waste aqueous solution.

Lead (II) nitrate is a white inorganic compound with molecular weight 331.2 g/mol. It was received from Merck, India and it was also used for the metal ions adsorption study.

Potassium dichromate is a hexavalent compound of chromium with molecular weight 294.185 g/mol. It was received from Merck, India and it was used to study the effectiveness of the hydrogel to adsorb positively charged species from water.

4.2.2. Methods

4.2.2.1. Synthesis of the mechanically tough hydrogel

The mechanically tough DN hydrogel was prepared through modification of our previously reported amphoteric hydrogel by eliminating the positive charge formation step as described in **Chapter 3**. Briefly, the aqueous solution of 2 g starch with 20 mL of

distilled water was stirred with a high-speed mechanical stirrer in a reactor. The temperature of the system was increased gradually up to 60 °C with a constant stirring until the starch was completely swelled and dispersed. Then, the calculated amount of ECH was mixed into it with the subsequent addition of 3N aqueous NaOH. The increase in viscosity indicates the formation of ECH cross-linked starch but the viscosity was not allowed to increase too high to prevent the formation of solid mass. Thereafter, N_2 gas was used to deoxygenate the reaction vassal followed by the addition of 2.10 g of AA, an aqueous solution of the initiator, APS (0.08 g), and the cross-linker, MBA (0.02 g), which were mixed by vigorous stirring. The reaction was allowed to proceed for another 1 h and thereafter, the desired amount of 8N aqueous solution of NaOH was added to neutralize the carboxylate groups of AA. Then the reaction mass was allowed to dry in a Teflon sheet to form the film. The amount of ECH was varied to prepare the hydrogels with three different degrees of cross-linking and encoded as SEAA1, SEAA2, and SEAA3. The compositions of the various constituents used in the formation of the hydrogels are given in **Table 4.1.** For comparison purposes, starch cross-linked with only ECH was prepared and encoded as SE. The hydrogel with only starch grafted PAA was also prepared as discussed in **Chapter 2** and coded as SAH 2.

Table 4.1. Amounts of reactants used in the synthesis process of the hydrogel.

Sample code	Starch content (g)	ECH content (g)	AA content (g)	MBA content (g)	APS content (g)
SEAA1	2	0.638	2.10	0.020	0.080
SEAA2	2	0.800	2.10	0.020	0.080
SEAA3	2	0.958	2.10	0.020	0.080
SE	2	0.958	.....	.....	.....
SAH 2	2	……..	2.10	0.020	0.080

4.2.3. Structural analysis

The FTIR spectra and XPS spectra of the synthesized hydrogel were recorded using the method and instrument as done in **Chapter 2**.

4.2.4. Determination of mechanical properties

The tensile strength measurements of the synthesized hydrogels were performed in a

Universal Testing Machine (Model WDW-10, Jinan, China) using 1.0 kN load cell at 10 mm min^{-1} crosshead speed.

4.2.5. Swelling study

The swelling ability of the synthesized hydrogel films was determined by using a similar method as described in **Chapter 2**.

4.2.6. Metal ion adsorption study

Desired amounts of the dry hydrogel films were immersed into the solutions containing lead (Pb^{2+}), nickel (Ni^{2+}), and copper (Cu^{2+}) ions at different concentrations under stirring conditions. After proceeding with adsorption, the metal ion-containing solutions were extracted at constant time intervals. An atomic adsorption spectrophotometer (AAS-ICE 3500, UK) was used to determine the residual metal ion concentrations and the same was applied to evaluate the metal ion adsorption capacity using **Eq. 3.1**.

where qe (mg g^{-1}) is the metal ion adsorption capacity at equilibrium, Co and Ce represent the initial and equilibrium metal ion concentrations (mg.mL^{-1}), M (mg) represents the hydrogel's weight, and V (mL) is the volume of metal ion solution used.

To explore the adsorption performance of the hydrogel under different conditions, factors like adsorbent dosages, pH, temperature, metal ion concentration, and adsorption time were varied. The adsorbent dosages for the metal ions were varied accordingly to the adsorption capacity of the adsorbent for each metal ion. The pH of the metal ion solution was varied from pH 2 to 7. Moreover, the adsorption capacity was investigated at room temperature (RT), at 313 K, and 323 K, while the metal ion concentration was varied from 30 ppm to 150 ppm. The equilibrium adsorption time for each metal ion were evaluated separately by determining the remaining metal ion concentration at different time intervals using an AAS.

Further, to check the recyclability of the hydrogel, after attaining the equilibrium adsorption, the adsorbent was washed with 0.1 N HCl solution and neutralized with NaOH for further use in the subsequent adsorption cycles. Again, the removal efficiency was measured in the same way by using the same AAS.

Moreover, to determine the adsorption performance for Cr (VI) ions, potassium dichromate solution was prepared in normal distilled water and also at different pH conditions (2, 4, 6, and 8), and after adsorption, Cr (VI) ion concentration is determined by using AAS.

To explore the performance of the hydrogel in practical conditions, actual wastewater are collected from the effluents of industries of Assam, India, and an adsorption experiment was done. However, the collected wastewater did not contain our studied metal ion and hence, we deliberately added in a very minute concentration (1.5 ppm). After adsorption, the water was collected and the remaining metal ion concentration was determined by using AAS, as done before.

4.3. Results and discussion

4.3.1. Synthesis of the mechanically tough hydrogel

To achieve mechanically tough hydrogel our previously reported amphoteric hydrogel was modified with the elimination of amphoteric properties along with enhancement of ECH cross-linking network (**Scheme 4.1.**).

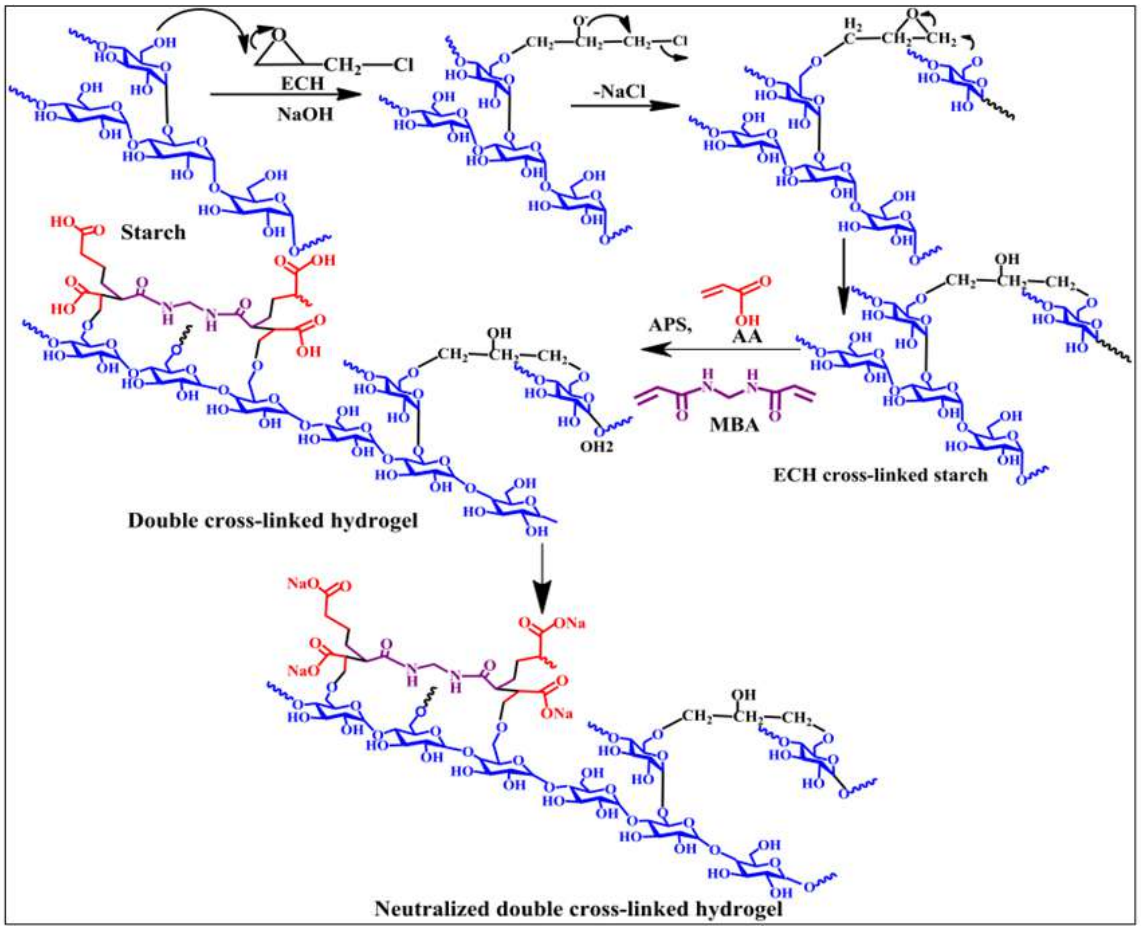

Scheme 4.1. Synthesis scheme and probable chemical structure of the hydrogel.

The modification drastically changes the chemical property of the synthesized hydrogel along with the changes in mechanical properties. The formation mechanism of the

hydrogel was consisting of two steps; in the first step, the epoxy ring of ECH was opened up in the presence NaOH and cross-linked with some of the primary hydroxyl groups of starch. Subsequently, in the second step, the remaining primary hydroxyl groups of ECH cross-linked starch were converted into primary radicals in the presence of initiator APS. Moreover, APS also initiates the free radical polymerization of AA. Meanwhile, vinyl groups of the second cross-linker, MBA reacted with AA chains to form a cross-linked structure in the starch backbone. Finally, the polymer chains were terminated upon depletion of all the monomers.

4.3.2. Structural analysis

4.3.2.1. FTIR spectral study

The FTIR spectra (**Figure 4.1.a** and **b**) provide supportive information for the reaction between ECH, starch, and AA moieties. The disappearance of the distinctive peaks of the ECH at 854.55 cm^{-1} (epoxy ring) and 760.75 cm^{-1} (C–Cl) in the FTIR spectrum of SE suggests the opening of epoxy ring and chemical reaction of it [11]. Further, it also gives evidence that ECH cross-linked on starch backbone through ether linkage. Moreover, the decrement of the strength of –OH stretching frequency of SE and all three SEAAs at 3436.60 cm^{-1} in comparison to the bare starch signifies the lowering of hydrogen bonding of the hydroxyl groups of starch, which in turn gives confirmation about the cross-linking between ECH and starch. For all SEAAs, the absorption bands at 2853.17–2924.46 cm^{-1} can be attributed to the C–H symmetric and asymmetric stretching frequencies, which are the important bands for starch and AA moiety [7].

Moreover, the band appeared at 1726.92 cm^{-1} representing the stretching frequency of carbonyl groups of PAA. The band appears at 1633.17 cm^{-1} for NH bending vibration which is the indication of successful cross-linking of MBA on PAA chains. The adsorption bands at 1407–1457.27 cm^{-1} attributed to the stretching frequency of $–H_2C–O–CH_2–$, which suggests that ether linkage was formed between starch's primary hydroxyl groups and PAA [12]. Moreover, it also supports that starch and ECH are connected through ether bonds, which was seen in the FTIR spectrum of SE. Additionally, the band appears around 1026 cm^{-1} due to the –C–O–C– linkage present in starch. All these results indicate the successful grafting of PAA moieties on ECH cross–linked starch.

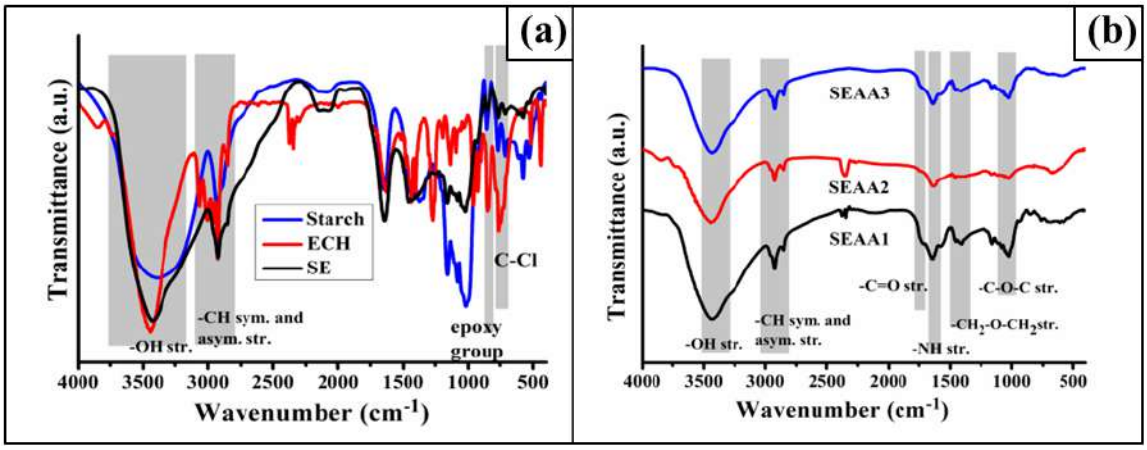

Figure 4.1. FTIR spectra of (a) ECH, Starch, and SE, and (b) SEAA1, SEAA2, and SEAA3.

4.3.2.2. XPS study

XPS analysis was conducted to verify the chemical composition of SEAA3 hydrogel (**Figure 4.2.a**). From the analysis, it was found that the hydrogel contains C (60.52%), N (1.22%), O (35.65%), and Na (2.61%). The indication of the conversion of the reaction was also investigated by the high-resolution XPS spectra of C 1s, O 1s, and N 1s (**Figure 4.2.b-d**). The deconvoluted C 1s peak of SEAA3 was attributed to (C–H and C–C), (C–N and C–O–C), (O–C–O, C–O, and C–O), and COO^- at binding energy of 284.66 eV, 285.70 eV, 286.12 eV, 288.10 eV, respectively [7, 13]. These are the characteristic peaks for the different carbon containing reactants such as starch, AA, MBA, and ECH. The high-resolution O 1s spectrum was deconvoluted into three peaks at 531.43 eV, 532.50 eV, and 533.10 eV which can be designated to (C–O, C–O–C), (O–C–O, and C=O) and COO^- groups, respectively.

Thus, from this analysis, the development of ether bonds between AA and starch as well as starch and ECH were confirmed. Moreover, the deconvoluted peaks for N at 399.90 eV and 400.44 eV for the presence of MBA inside the hydrogel [13]. Further, the XPS spectrum also confirmed the presence of Na (**Figure 4.2.e**), which was used to neutralize the COO^- groups of PAA. Thus, XPS analysis informed about the elemental composition and provides idea on the chemical structure of the synthesized hydrogel.

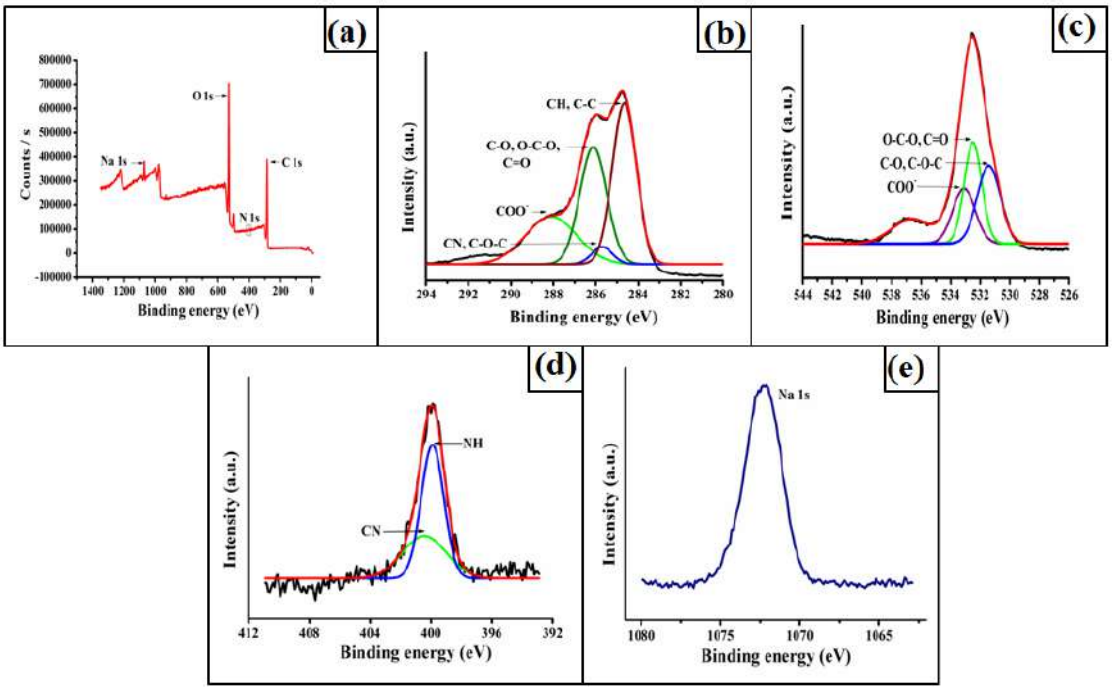

Figure 4.2. XPS spectra of (a) SEAA3, (b) C 1s, (c) O 1s, (d) N 1s, and (e) Na 1s.

4.3.3. Mechanical properties

The as-prepared hydrogel possesses outstanding mechanical strength due to the presence of DN cross-linking. **Figure 4.3.a** depicts the stress–strain curves for SEAA1, SEAA2, and SEAA3. The mechanical strength of SEAA1 found to be 0.63±0.33 MPa and but the same was increased up to 2.78±0.58 MPa in case of SEAA3. This result clearly indicates that the increasing amount of cross-linker ECH causes the enhancement of the tensile strength of the hydrogels [3]. This is due to the introduction of the second cross-linking network, which contributed towards the dissipation of applied energy and can tolerate the applied stress [3]. Thus, the hybrid DN can contribute to the increment of mechanical strength of the hydrogel. The enhancement of the mechanical strength of the hydrogel with the increase in the amount of the cross-linker also supports this fact. Further, the digital photographs of **Figure 4.3.(b-e)** provide evidence for the mechanical strength of the hydrogel. From these figures, it is clearly observed that the prepared hydrogel possesses extraordinary toughness and has the ability to overcome the brittleness of the conventional mono cross-linked hydrogel. However, the elongation of the hydrogel decreases with the increase in ECH amount i.e., with the increase in the cross-linking density in the resulting hydrogel. The reduction of elongation ratio with the increase in cross-linker amount was also found by Lin et al. [6].

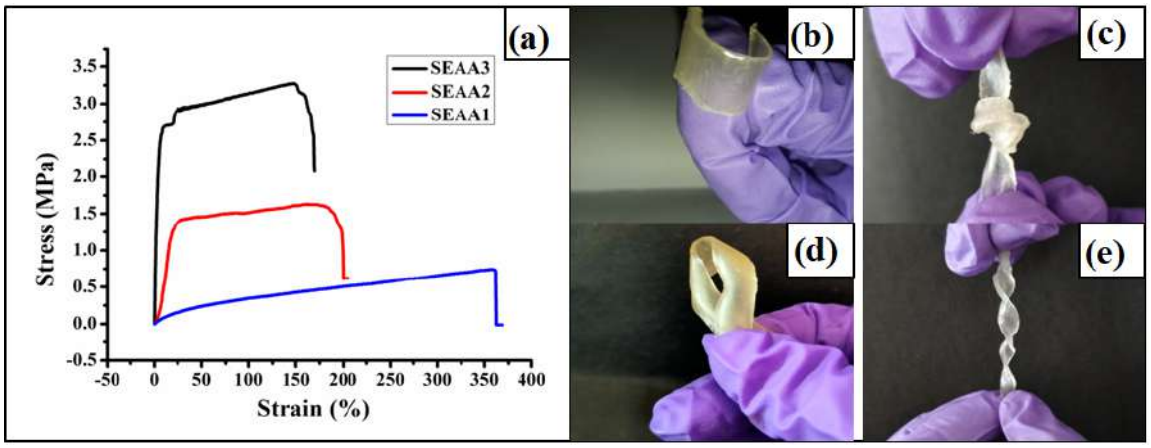

Figure 4.3. (a) Stress-strain curves of the hydrogels; and (b)–(e) photographs showing the evidence for the toughness of the hydrogel.

4.3.4. Swelling study

Figure 4.4. shows the swelling behaviors of the synthesized hydrogels. The water absorption capacity of the hydrogel was found to be much lower than the other conventional hydrogels, although it contains a hydrophilic PAA moiety. This result revealed that the increase of cross-linking density drastically decreases the swelling capacity. In this vein, ECH as a cross-linker enhances the cross-linking density in the polymeric matrix and thereby increasing the toughness of the hydrogel.

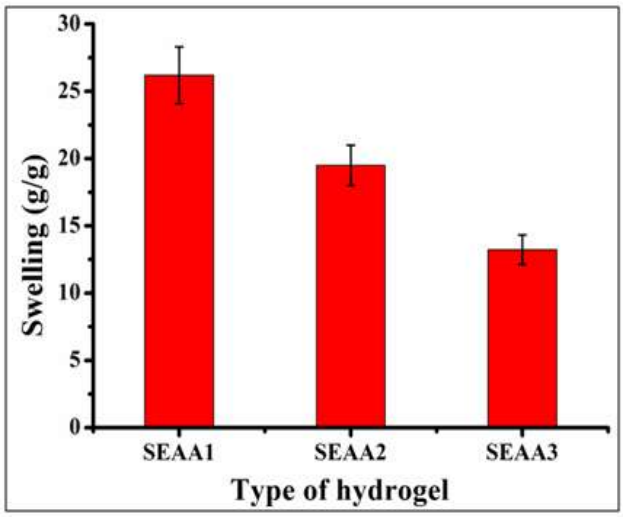

Figure 4.4. Swelling ability of the hydrogels.

The high mechanical strength of the hydrogel also does not allow to open up the gel too much, which results in a decrease in water absorption capacity [12]. Moreover, the

swelling ability decreased with the increase of ECH content, which also supports that the double cross-linking network is responsible for this low value of swelling.

4.3.5. Metal ion adsorption study

A liquid-phase metal ion adsorption experiment was conducted to explore the adsorption behavior of the hydrogel. **Figure 4.5.** displays the metal ion adsorption potential of the synthesized hydrogel for Pb^{2+}, Ni^{2+} and Cu^{2+} ions. As expected, the adsorption performance of SEAA1 is slightly greater than SEAA2 and SEAA3 and this is due to higher ECH content, which decreases the amount of active anionic groups, in the same amount of hydrogel. But the difference was not too much as the difference in amount of ECH was not very high and hence the anionic carboxylate groups did not differ too much. As the adsorption efficiency was not differed too much hence, by considering the combined effects of the tensile strength value and the favorable adsorption capacity, the SEAA3 was chosen for further experiment. It is well established that the removal performance of an adsorbent from the aqueous solution of adsorbate is mainly dependent on adsorbent dosages, temperature, solution pH, equilibrium time of adsorption and initial concentration of metal ions, etc. To achieve the best result, the effects of these parameters were investigated thoroughly.

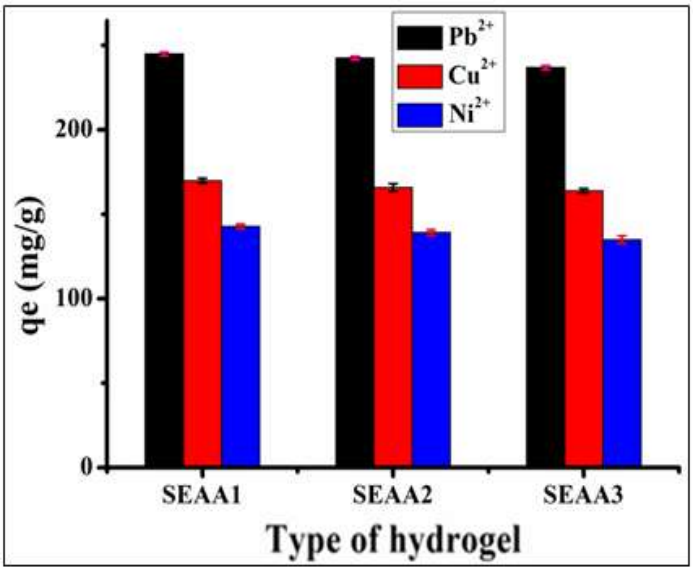

Figure 4.5. Metal ion adsorption capacity of all three compositions of the hydrogels, (metal ion concentration 150 ppm, 50 mL; pH: 5, temperature 323 K, adsorbent dosage: 30 mg for Pb^{2+}, 40 mg for $Cu^{2+,}$ and 50 mg for Ni^{2+}).

4.3.5.1. Effect of adsorbent dosages

The effect of adsorbent on the metal ion adsorption capacity was evaluated to obtain the optimum hydrogel dosages for the removal of each metal ion (**Figure 4.6.a** and **b**).

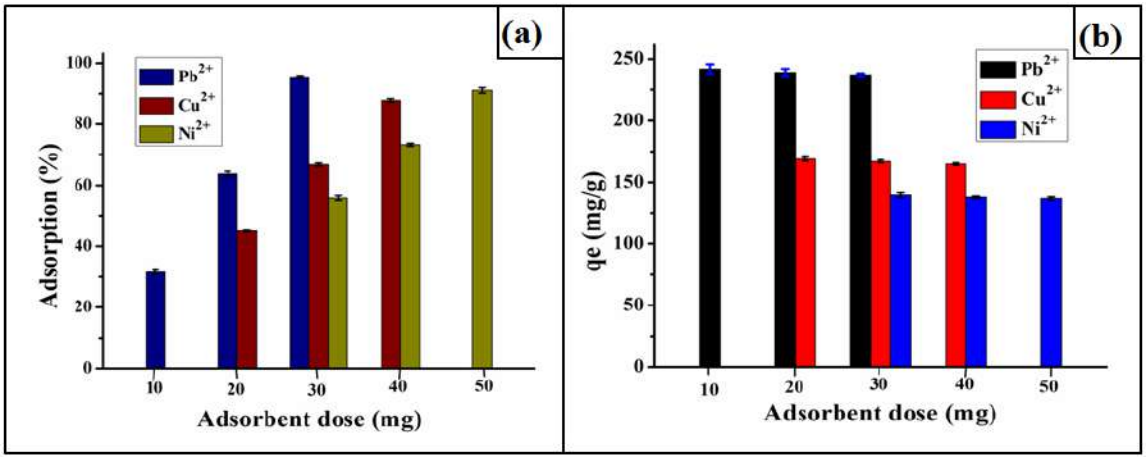

Figure 4.6. (a) Effect of adsorbent dosages on adsorption for the metal ions, and (b) effect of adsorbent dosages on adsorption amount for metal ions (metal ion concentration 150 ppm, 50 mL; pH: 5, temperature 323 K, adsorbent dosage: 30 mg for Pb^{2+}, 40 mg for $Cu^{2+,}$ and 50 mg for Ni^{2+}).

It is seen that the adsorption amount per g (qe) of the adsorbent decreased with the increase in adsorbent dosages, but the corresponding adsorption percentage increased. The maximum adsorption percentage for Pb^{2+}, Cu^{2+}, and Ni^{2+} was found to be 95.53%, 87.85%, and 91.06% with adsorbent dosages of 30 mg, 40 mg, and 50 mg, respectively. Hence, combining both these results, the adsorbent dosages for the metal ions were optimized such that more than 85% metal can be removed for a metal ion concentration of 150 ppm. Moreover, from the effect of adsorbent dosages, the adsorption amount of SEAA3 for the three metal ions are found to be 237.41±1.2 mg/g, 164.72±1.08 mg/g, 136.6±1.32 mg/g for Pb^{2+}, Cu^{2+}, Ni^{2+} respectively. This observation is due to the highest affinity of Pb^{2+} for carboxyl groups followed by the other two ions [14].

4.3.5.2. Effect of pH

The solution pH is a significant variable that greatly influences the adsorption performance. The solution pH can influence both the physico-chemical behavior of the adsorbent and the nature of metal ions in an aqueous solution [15]. The influence of pH on metal ions adsorption by SEAA3 was investigated over the pH range, from 2 to 7 and the effects are presented in **Figure 4.7.a**. The adsorption capacity increased with the raise in solution pH from 2 to 5 and subsequently diminished. The relatively lower

adsorption performance at pH < 5 is due to the competitive effect between metal ions and the huge amount of H^+ ions to interact with the negatively charged active sites (COO^-) of the adsorbent. With an increase in pH, there was a significant rise in adsorption efficiency, due to the lowering of H^+ ions in the solutions which decreased the competition between the metal ions and H^+ ions. However, further increases in solution pH decreased the adsorption efficiency, because of the presence of plenty of HO^- ions in the medium that enhance the adsorbate affinity towards them resulting in a decreased efficiency of the adsorbent for metal ions binding [8].

4.3.5.3. Effect of temperature

The temperature has a notable effect on adsorption. The adsorption performance of SEAA3 was enhanced in the case of all three metal ions with a rise in temperature from RT to 323 K (**Figure 4.7.b**). At elevated temperatures, swelling allows the passage of huge numbers of metal ions inside the hydrogel matrix. However, in contact with water, all the adsorbates may or may not enter inside the adsorbent, which depends on the extent of interaction between them. But with the increase in temperature, large numbers of metal ions can gain the required energy to interact with the negatively charged adsorbent sites. Besides this, an increase in temperature also enhanced the diffusion rate by lowering the solution viscosity resulting in a superior rate of adsorption. This proves the endothermic behavior of the adsorption process [16].

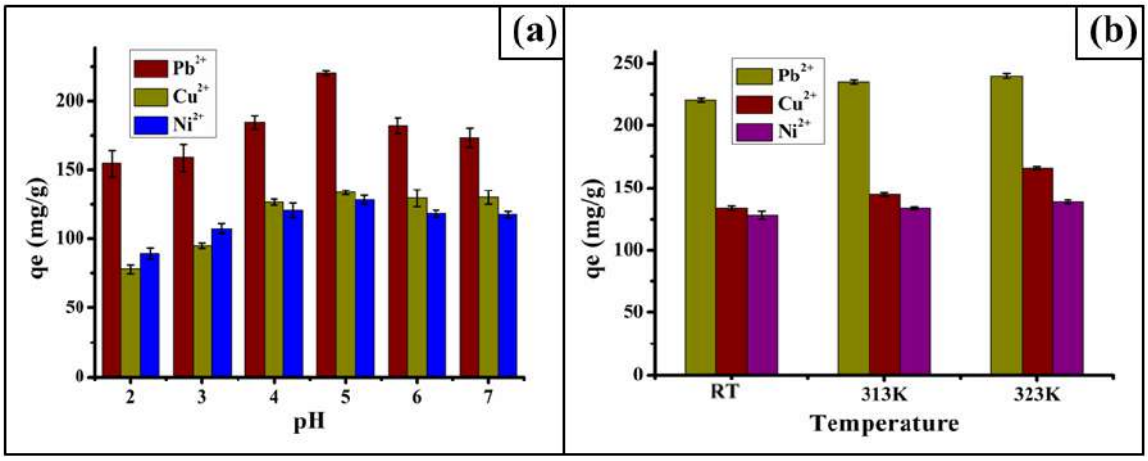

Figure 4.7. (a) Effect of pH (RT), and (b) effect of temperature (metal ion concentration 150 ppm, 50 mL; pH: 5, temperature 323 K, adsorbent dosage: 30 mg for Pb^{2+}, 40 mg for $Cu^{2+,}$ and 50 mg for Ni^{2+}).

4.3.5.4. Effect of contact time

Figure 4.8.a demonstrated the changes in adsorption amount with time. It is seen that the initial rate of metal ion uptake increased with time and attain a maximum within 35 min for Pb^{2+} and Cu^{2+}, while only 30 min is required for Ni^{2+}, after which the values are leveled off. At the initial state, the rate of adsorption is much higher than in the equilibrium state. This result indicates that at the first stage, there is electrostatic interaction of the negatively charged active sites with the metal ions. But within a few minutes, the active adsorbent sites decrease for metal ions which reduce the rate of adsorption. This result indicates that the synthesized hydrogel can achieve equilibrium adsorption within a very short time, and this is a very useful quality of an adsorbent for practical applications.

4.3.5.5. Effect of initial metal ion concentration

To investigate the performance of the adsorbent the concentration of metal ions changes from 30 ppm to 150 ppm. The adsorption amount (qe) increased with the increase in metal ions concentration (**Figure 4.8.b**), but the corresponding percentage of adsorption was found to be declined (**Figure 4.8.c**). A higher adsorption percentage was monitored at a lower adsorbate concentration (30 ppm) due to the availability of an abundance of active adsorption sites. In contrast, the increased metal ion concentration lowers the available active adsorption sites resulting lowering adsorption percentage [17].

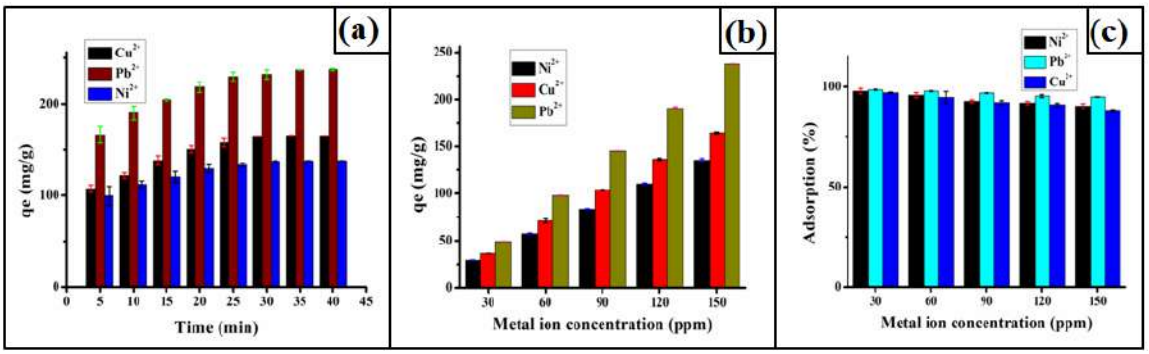

Figure 4.8. (a) Effect of time on amount of adsorption, (b) effect of metal ion concentration on amount of adsorption, and (c) effect of metal ion concentration on adsorption (metal ion concentration 150 ppm, 50 mL; pH: 5, temperature 323 K, adsorbent dosage: 30 mg for Pb^{2+}, 40 mg for $Cu^{2+,}$ and 50 mg for Ni^{2+}).

4.3.5.6. Kinetics of adsorption

To understand the dynamics and rate of adsorption, kinetics study is of utmost

importance. Here different kinetics models such as pseudo-first-order pseudo-second-order, and intra-particle diffusion are also studied as discussed in **Chapter 3** (**Figure 4.9.a-c**) [18, 19]. Likewise, the dye adsorption and metal ion adsorption also followed pseudo-second-order kinetics with a high correlation factor (**Table 4.2.**).

Table 4.2. The parameters related to kinetics for Pb^{2+}, Cu^{2+}, and Ni^{2+} ions adsorption on SEAA3.

Model	**Kinetic parameters**	**Ni^{2+} ions**	**Cu^{2+} ions**	**Pb^{2+} ions**
Pseudo- first order	k_1	1.54×10^{-1}	1.51×10^{-1}	1.51×10^{-1}
	R^2	0.8407	0.8397	0.8534
Pseudo-second order	K_2	4.7×10^{-2}	3.45×10^{-2}	3.4×10^{-2}
	R^2	0.9988	0.9976	0.9989
Intra-particle diffusion	K_3	9.79	15.17	17.84
	C	81.35	77.06	133.16

The low correlation factor for the pseudo-first-order kinetics suggests the unfavorability of this model, which further gives evidence for the occurrence of ionic interaction between the adsorbate and adsorbent. It also designates that the adsorption proceeded through electron transfer, share, or exchange between the metal ions and the hydrogel [20,12]. Moreover, the intra-particle diffusion model of the metal ions adsorption showed multi-linearity (**Figure 4.9.c)**. These linear regions indicate that more than one process simultaneously affected the adsorption process. The first region has the largest diffusion rate, and it is interrelated to the diffusion of the metal ions to the external layer of the adsorbent through the aqueous solution. The second region has a relatively lower adsorption phase corresponding to the internal diffusion of the adsorbate inside the pores of the adsorbent. With an extension of time, concentrations of metal ions come down to a lower value and most of the active adsorption sites were occupied by the adsorbents. Hence, the third stage has a nominal diffusion rate. During the whole adsorption process, none of the plots passes through the origin indicating the involvement of some other mechanisms. Moreover, the presence of a large value of intercept indicates the thickness of the boundary layer of the adsorbent. Thus, it can be concluded that surface adsorption is also taking place along with intra-particle diffusion [21, 22]. All the kinetics data showed good agreement with the kinetics study of dye adsorption as discussed in

Chapter 3. Thus, from the kinetics study, it can be concluded that the solid-liquid adsorption processes proceed through the three-stage path. In the first step, the metal ions transport from the bulk aqueous solution to the exterior adsorbent's surface. After that the metal ions transport to the hydrogel's interior part. Finally, in the third step, electrostatic interaction occurs between the positively charged metal ions and the hydrogel. Thus, in conclusion, along with surface adsorption, there is penetration of metal ions toward the interior parts of the hydrogel surface [21,22].

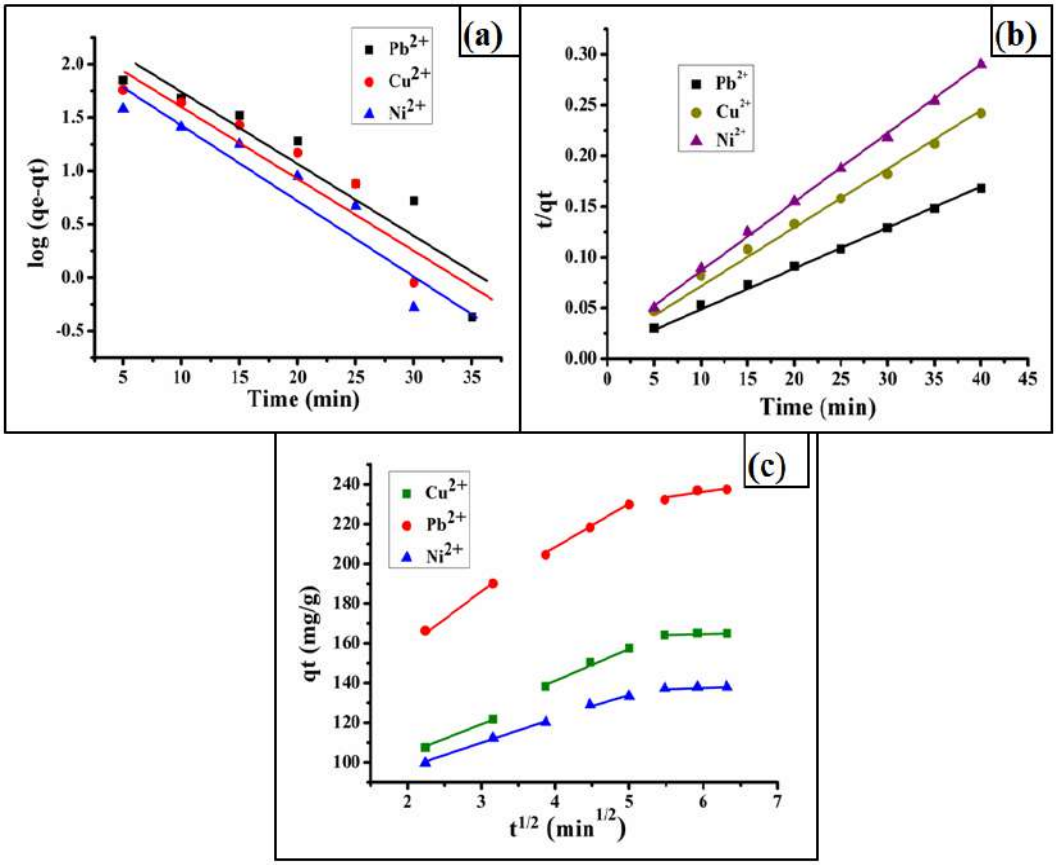

Figure 4.9. (a) Pseudo-first order kinetics, (c) pseudo-second order kinetics, and (d) intra-particle diffusion kinetics model for Pb^{2+}, Cu^{2+}, and Ni^{2+} (metal ion concentration 150 ppm, 50 mL; pH: 5, temperature 323 K, adsorbent dosage: 30 mg for Pb^{2+}, 40 mg for Cu^{2+}, and 50 mg for Ni^{2+}).

4.3.5.7. Isotherm study of adsorption

As discussed in **Chapter 3**, the adsorption isotherms provide qualitative information on the adsorption capacity and also the nature of the interaction between adsorbate and adsorbent. Moreover, they also provide information on the equilibrium concentration of the adsorbate. Likewise, the dye adsorption, Langmuir, and Freundlich adsorption

isotherms are also used to explain the experimental data (**Figure 4.10.**(**a** and **b**)). The smaller correlation coefficient value of Langmuir adsorption isotherm indicates the unfavorability of the model, which proves that the multilayer adsorption occurred during metal ion uptake (**Table 4.3.)**. However, the experimental data fitted well with the Freundlich isotherm and also demonstrated the multilayer adsorption process [20,23]. The 1/n value obtained from the slope of this model indicates the chemisorption between the adsorbate and adsorbent [12] and this result also concluded that the metal ion adsorbed through electrostatic interaction on the synthesized hydrogel (**Table 4.3.**).

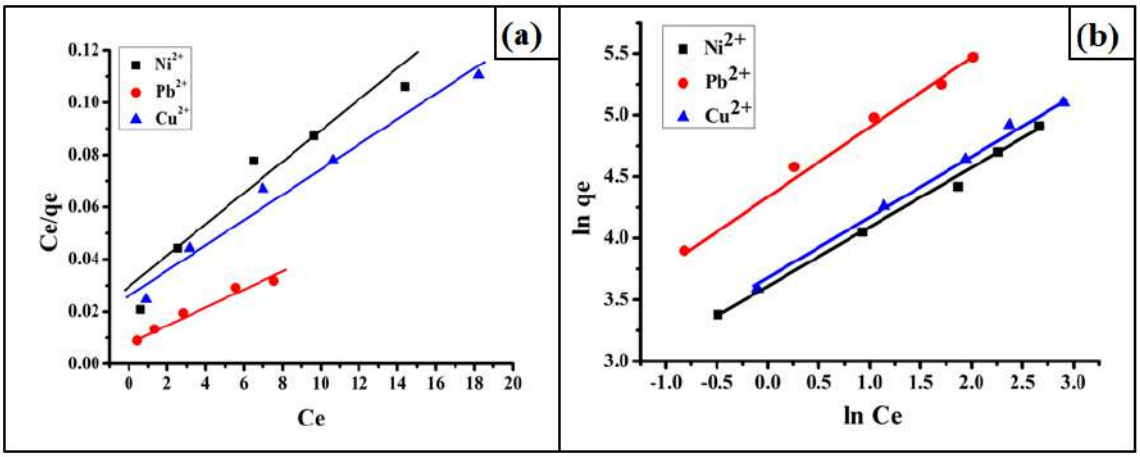

Figure 4.10. (a) Langmuir adsorption isotherm, and (b) Freundlich adsorption isotherm for Pb^{2+}, Cu^{2+}, and Ni^{2+} (metal ion concentration 150 ppm, 50 mL; pH: 5, temperature 323 K, adsorbent dosage: 30 mg for Pb^{2+}, 40 mg for Cu^{2+}, and 50 mg for Ni^{2+}).

Table 4.3. The parameters related to the isotherms model for Pb^{2+}, Cu^{2+}, and Ni^{2+} ions adsorption on SEAA3.

Model	**Kinetic parameters**	**Ni^{2+} ions**	**Cu^{2+} ions**	**Pb^{2+} ions**
Langmuir Isotherm	q_m	166.67	210.52	312.5
	K_L	4.45	5.68	2.81
	R^2	0.9157	0.9675	0.9619
Freundlich Isotherm	n	2.09	1.96	1.85
	K_F	36.60	38.47	79.84
	R^2	0.9930	0.9954	0.9924

4.3.5.8. Metal ions adsorption-desorption studies

To render the adsorption process economically viable as well as environmentally friendly, the adsorbent should possess excellent recyclability. An efficient adsorbent should have both high adsorption capacity along with prominent desorption capacity. Most importantly reusability of any material for practical applications is very promising if it is endowed with fantastic mechanical properties. A mechanically tough hydrogel can be easily removed after adsorption and the absorbent can be used for several purification cycles. Due to the high mechanical strength of our synthesized SEAA3 hydrogel, it could be easily recycled without disintegrating as shown in **Figure 4.11.(a-c)**. In **Figure 4.11.(d-f)**, the images of the disintegrated SAH 2 hydrogel after metal ions adsorption are shown. Moreover, the hydrogel could be rapidly desorbed the metal ions after treatment with the 0.1N HCl solution only for 5–10 min and could be reused for the subsequent cycles. In an acidic medium, the active sites of the adsorbents are protonated by H^+ ions of HCl, which decreases the electrostatic interaction between the adsorbent and the positively charged metal ions. **Figure 4.11.(g** and **h)** shows the removal efficiency along with the subsequent adsorption capacity. To recognize the recyclability of SEAA3, three adsorption-desorption cycles were carried out and after 3rd cycle, 92.67%, 90.8%, and 89.36% desorption results were found for Cu^{2+}, Ni^{2+}, and Pb^{2+} ions, respectively (**Figure 4.11.g** and **h**).

Moreover, the adsorption percentage decreases from 94.97%, 87.78%, and 91.78% to 79.04%, 80.57%, and 87.37% in the case of Pb^{2+}, Cu^{2+}, and Ni^{2+}, respectively (**Figure 4.11.h**). These results concluded that SEAA3 hydrogel is a prominent recyclable adsorbent for metal ions. However, after each cycle desorption capacity and adsorption efficiency slightly deteriorated because of the residual metal ions occupying the active adsorption sites.

4.3.5.9. Study on Cr (VI) adsorption

The study on the adsorption of Cr (VI) was carried out and found that the synthesized hydrogel showed negligible adsorption (2.57 mg/g) for the Cr (VI) ions. The electrostatic interaction between the negatively charged hydrogel and the positively charged metal ion is the predominant cause of metal ions adsorption. But as Cr (VI) exists as an anion ($Cr_2O_7^-$) in an aqueous solution [24], there is electrostatic repulsion with the negatively charged adsorbent, resulting in poor adsorption. The slight adsorption may be due to

physical entrapment in the void of the hydrogel during swelling and the hydrogen bonding interaction with the hydroxyl groups present in the hydrogel.

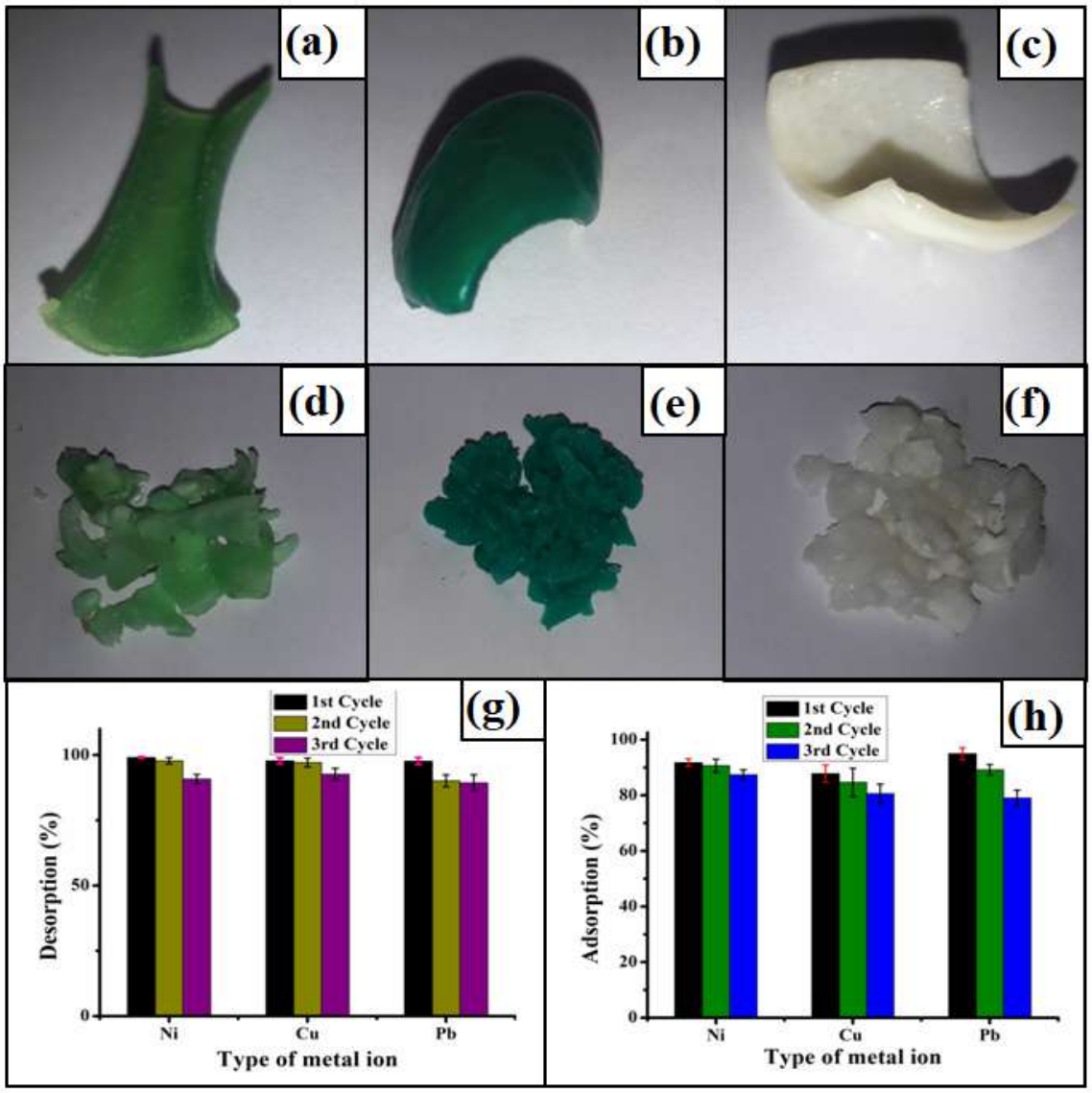

Figure 4.11. (a) Photographs of SEAA3 after metal ions adsorption (a) Ni^{2+}, (b) Cu^{2+} and (c) Pb^{2+}; Metal ion adsorbed SAH 2 (d) Ni^{2+}, (e) Pb^{2+}, and (f) Cu^{2+}; (g) Metal ion desorbed after each cycle and (h) Adsorption of metal ion in each cycle.

Figure 4.12.(**a** and **b**) presents the potassium dichromate solution before and after adsorption respectively. After the adsorption experiment, no distinct color change was observed. **Figure 4.12.c** depicts the slight adsorption capacity of SEAA3 for Cr (VI) ion. The effect of pH on the adsorption of Cr (VI) was investigated at different pH values (pH 2, 4, 6, and 8). The results showed that the adsorption capacity was affected greatly by the pH values. The adsorption capacity was found to be the highest at pH 2 and decreased with an increase in pH value (**Figure 4.12.d**). Under low pH values, the

predominant presence of H^+ ions makes the carboxylate groups of AA and Cr (VI) ions exist mainly as $HCrO_4^-$ ions. Thus, the repulsion between the negatively charge COO^- groups and the $HCrO_4^-$ ions decreased significantly. On the other hand, with the increase in pH values H^+ ions concentrations decreased and concentrations of OH^- ions increased. This leads to an increment of electrostatic repulsion with negatively charged ions which results in the lower adsorption capacity [24].

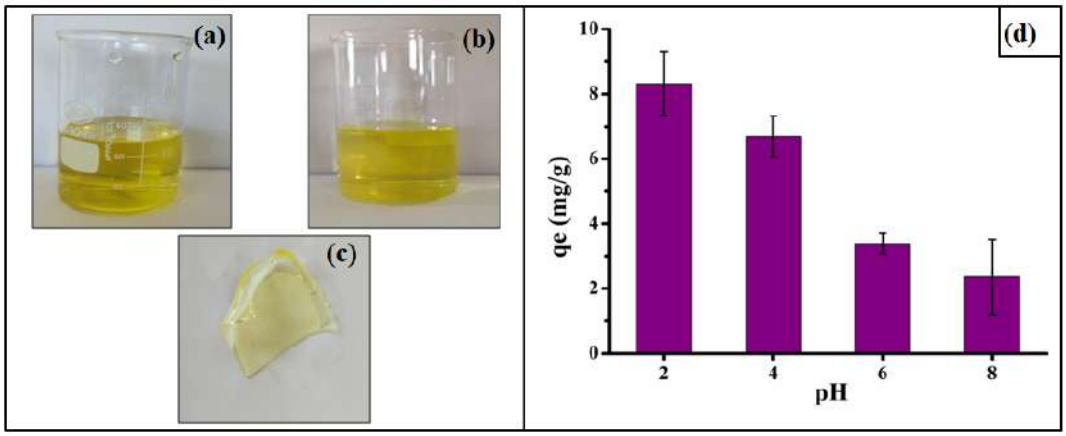

Figure 4.12. (a) Potassium dichromate solution before adsorption, (b) Potassium dichromate solution after adsorption, (c) Cr (VI) adsorbed SEAA3, and (d) effect of pH on Cr (VI) adsorption.

4.3.5.10. Treatment of actual industrial wastewater

The adsorption performance of the hydrogel was investigated in actual wastewater too. After the treatment with SEAA3 the adsorption capacity for Cu^{2+} and Pb^{2+} was found to be 94.67% and 100%, respectively, while for Ni^{2+} it was found to be 92.67%. Thus, this result showed that the synthesized hydrogel can also be able to show its adsorption performance even in actual wastewater, not only in laboratory-generated wastewater. Laboratory-generated wastewater is produced using distilled water, but industrial waste contains various other contaminants. Our hydrogel can show its efficiency with these contaminants. Moreover, the hydrogel can also be able to adsorb the metal ions in very low concentrations, which is one of the most important requirements for practical wastewater treatment plants. Thus, these results showed that the hydrogel is suitable for actual wastewater treatment and hence it could be used in a practical wastewater purifier.

4.3.5.11. Metal ion adsorption mechanism

The kinetics and the isotherm studies revealed that the adsorption of metal ions on the synthesized adsorbent occurred predominantly through the ionic bond formation. Further, to investigate the adsorption mechanism, participation of functional groups, and the adsorbent's chemical state before and after adsorption, XPS analysis was carried out on metal ion adsorbed SEAA3. XPS analysis is often used to understand the interaction between metal ions and the active adsorbent sites because the chemical bonding formed between a metal ion and the adsorbent can cause changes in electron distribution around the particular atoms. The interaction of electron-donating groups can cause a lowering in the binding energy, while electron-withdrawing groups raise the binding energy [25]. **Figure 4.13.a** shows the changes in the chemical composition of SEAA3 after Cu^{2+} adsorption. After the adsorption of Cu^{2+}, the Na 1s peak disappeared from SEAA3 (**Figure 4.2.a**), instead, the characteristics peaks for Cu^{2+} were observed (**Figure 4.13.b**). The disappearance of Na peaks confirmed the ion exchange between the $–COONa^{+}$ groups of the hydrogel and the metal ions. There are two peaks for Cu^{2+} are observed at binding energies of 933 and 952.9 eV, which corresponded to Cu $2p_{3/2}$ and Cu $2p_{1/2}$, respectively. Moreover, these Cu $2p_{3/2}$ and Cu $2p_{1/2}$ peaks can be further deconvoluted which represents the coordinative interaction of Cu^{2+} with the hydroxyl groups of starch and the ionic bonding of the metal ions with the carboxylate ions of PAA. Moreover, the presence of the satellite peaks in the spectrum gives evidence for the +2 oxidation state of Cu [13]. In addition to this, after Cu^{2+} adsorption, the C 1s and O 1s peak positions were also changed. The deconvoluted C 1s peak at 264.12 eV was shifted to 264.10 eV, probably due to the interaction of metal ion with the C–OH group of the adsorbent, while the 288.10 eV was shifted to higher binding energy (**Figure 4.13.c**). This is because of the binding of Cu^{2+} ions to the $COO^{–}$ groups of the adsorbent. Moreover, the O 1s peak was also shifted to higher binding energy (**Figure 4.13.d**), which indicates the interaction of the metal ion with oxygen atoms, which results in the reduction of electron density of the adsorbent [13]. Thus, XPS spectra provide the evidence for successful adsorption of Cu^{2+} ions on the adsorbent and the interactive mood predominantly through ion exchange between the metal ions and the Na^{+} ions of $COO^{–}$.

Moreover, XPS analysis was also performed on Ni^{2+} adsorbed SEAA3 and Pb^{2+} adsorbed SEAA3 (**Figure 4.14.a** and **b**). These figures clearly provide information about the presence of Ni^{2+} and Pb^{2+} ions in the spectra. The Ni $2p_{3/2}$ and Ni $2p_{1/2}$ peaks are observed at the binding energies of 855.5 eV and 873.6 eV, respectively [26]. Further,

these peaks can be deconvoluted to obtain four peaks, as shown in **Figure 4.14.c**.

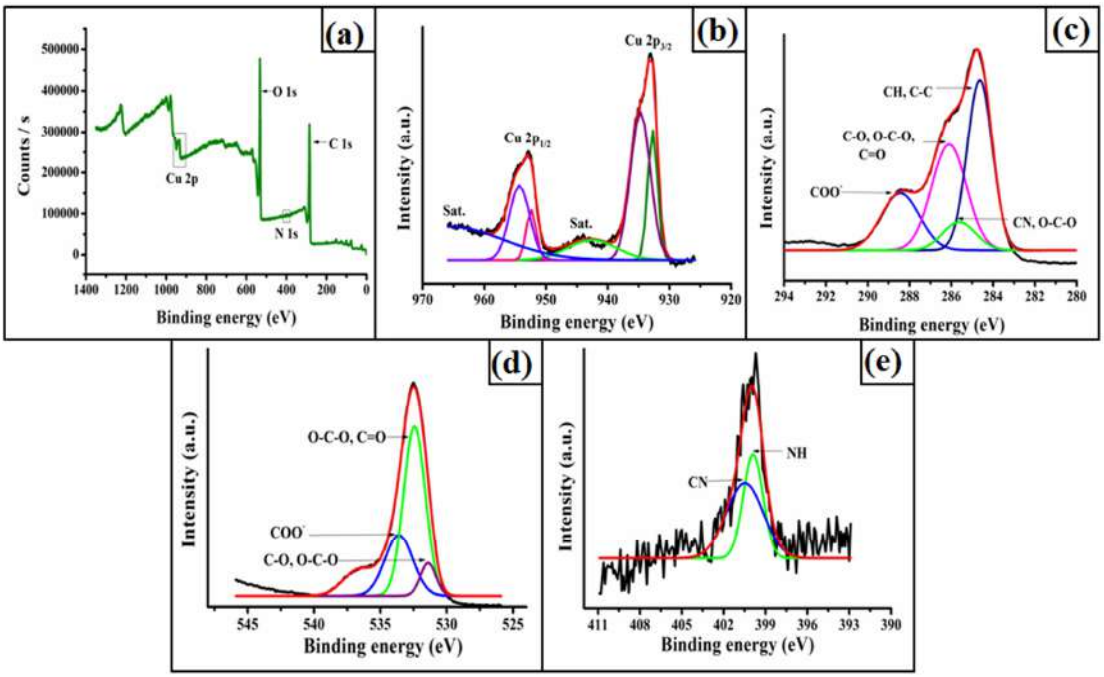

Figure 4.13. (a) XPS spectrum of SEAA3-Cu^{2+}, (b) Cu $2p_{3/2}$ and Cu $2p_{1/2}$ peaks, (c) C 1s peaks, (d) O 1s peaks, and (e) N 1s peaks for SEAA3-Cu^{2+}.

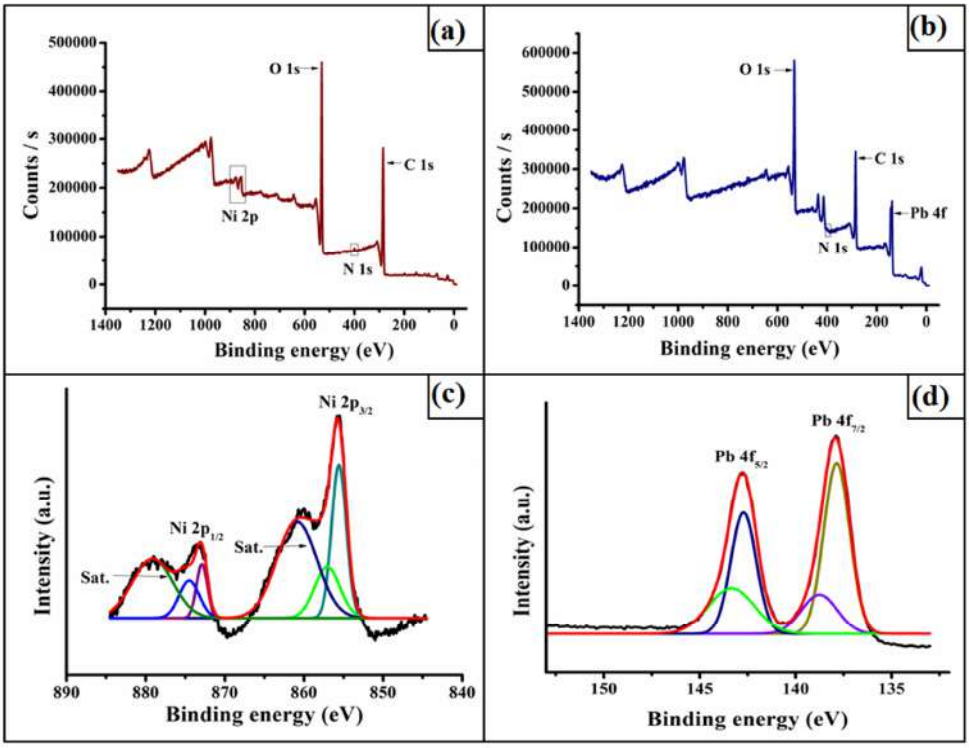

Figure 4.14. (a) XPS spectrum of SEAA3-Ni^{2+}, (b) XPS spectrum of SEAA3-Pb^{2+}, (c) Ni $2p_{3/2}$ and Ni $2p_{1/2}$ peaks, and (d) Pb $4f_{7/2}$ and Pb $4f_{5/2}$ peaks.

Moreover, the satellite peaks are also present in the spectrum. In a similar manner, the Pb4$f_{7/2}$ and Pb 4$f_{5/2}$ peaks are found at 137.9 eV and 142.7 eV, which can also be deconvoluted into four peaks, as shown in **Figure 4.14.d** [27]. These peaks correspond to the interaction of the metal ions with the starch hydroxyl groups and carboxylate groups of PAA. The schematic representation of the metal ion adsorption on the synthesized hydrogel is shown in **Scheme 4.2**.

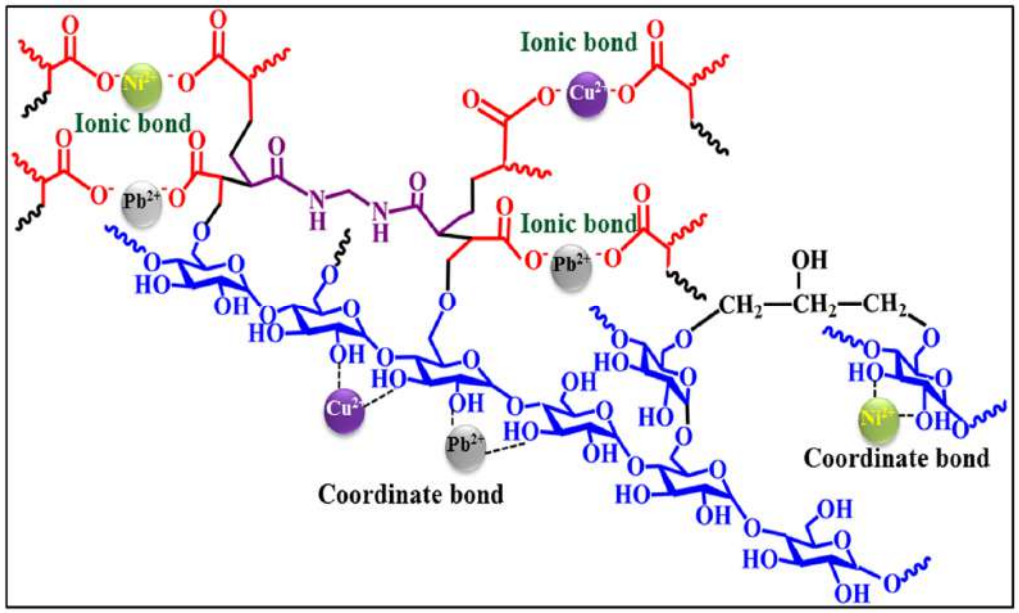

Scheme 4.2. Schematic representation for the interactions of metal ions with the adsorbent.

4.4. Conclusion

The work demonstrated a facile way to introduce a double cross–linked network on the starch backbone and reported a hydrogel with high mechanical strength. The introduction of the double cross-linked network results in an effective enhancement of the mechanical strength up to 2.78±0.58 MPa for the hydrogel. In addition to this, the hydrogel showed noteworthy performance for wastewater treatment with the potential to adsorb toxic heavy metal ions. The adsorption phenomenon is well-fitted by the Freundlich adsorption model and follows pseudo-second-order kinetics. More importantly, the excellent mechanical strength allows the hydrogel with many extraordinary properties like rapid separation and outstanding recyclability. In summary, our synthetic strategy not only provides a novel hydrogel with outstanding mechanical properties but also offers a recyclable adsorbent for heavy metal ions adsorption from wastewater. This

research work promotes the existing hydrogel research for the development of high-performing mechanically tough hydrogel with pollutants removal ability.

References

[1] Cui, W., Ji, J., Cai, Y. F., Li, H., and Ran, R. Robust, anti-fatigue, and self-healing graphene oxide/hydrophobically associated composite hydrogels and their use as recyclable adsorbents for dye wastewater treatment. *Journal of Materials Chemistry A*, 3(33):17445-17458, 2015.

[2] Sun, J. Y., Zhao, X., Illeperuma, W. R., Chaudhuri, O., Oh, K. H., Mooney, D. J., and Suo, Z. Highly stretchable and tough hydrogels. *Nature*, 489(7414):133-136, 2012.

[3] Gong, Z., Zhang, G., Zeng, X., Li, J., Li, G., Huang, W., and Wong, C. High-strength, tough, fatigue resistant, and self-healing hydrogel based on dual physically cross-linked network. *ACS Applied Materials & Interfaces*, 8(36):24030-24037, 2016.

[4] Ali, I. New generation adsorbents for water treatment. *Chemical Reviews*, 112(10):5073-5091, 2012.

[5] Yang, C. H., Wang, M. X., Haider, H., Yang, J. H., Sun, J. Y., Chen, Y. M., and Suo, Z. Strengthening alginate/polyacrylamide hydrogels using various multivalent cations. *ACS Applied Materials & Interfaces*, 5(21):10418-10422, 2013.

[6] Lin, P., Ma, S., Wang, X., and Zhou, F. Molecularly engineered dual-crosslinked hydrogel with ultrahigh mechanical strength, toughness, and good self-recovery. *Advanced Materials*, 27(12):2054-2059, 2015.

[7] Sarmah, D. and Karak, N. Double network hydrophobic starch based amphoteric hydrogel as an effective adsorbent for both cationic and anionic dyes. *Carbohydrate Polymers*, 242:116320, 2020.

[8] Ma, J., Zhou, G., Chu, L., Liu, Y., Liu, C., Luo, S., and Wei, Y. Efficient removal of heavy metal ions with an EDTA functionalized chitosan/polyacrylamide double network hydrogel. *ACS Sustainable Chemistry & Engineering*, 5(1):843-851, 2017.

[9] Ahamad, T., Naushad, M., Mousa, R. H., and Alshehri, S. M. Fabrication of starch-salicylaldehyde based polymer nanocomposite (PNC) for the removal of

pollutants from contaminated water. *International Journal of Biological Macromolecules*, 165:2731-2738, 2020.

[10] Alhokbany, N., Ahamad, T., Naushad, M., and Alshehri, S. M. Feasibility of toxic metal removal from aqueous medium using Schiff-base based highly porous nanocomposite: Adsorption characteristics and post characterization. *Journal of Molecular Liquids*, 294:111598, 2019.

[11] Song, Y., Li, L., and Zheng, Q. Influence of epichlorohydrin modification on structure and properties of wheat gliadin films. *Journal of Agricultural and Food Chemistry*, 57(6):2295-2301, 2009.

[12] Sarmah, D. and Karak, N. Biodegradable superabsorbent hydrogel for water holding in soil and controlled-release fertilizer. *Journal of Applied Polymer Science*, 137(13):48495, 2020.

[13] Zhang, M., Song, L., Jiang, H., Li, S., Shao, Y., Yang, J., and Li, J. Biomass based hydrogel as an adsorbent for the fast removal of heavy metal ions from aqueous solutions. *Journal of Materials Chemistry A*, 5(7):3434-3446, 2017.

[14] An, B., Lee, H., Lee, S., Lee, S. H., and Choi, J. W. Determining the selectivity of divalent metal cations for the carboxyl group of alginate hydrogel beads during competitive sorption. *Journal of Hazardous Materials*, 298:11-18, 2015.

[15] Xu, R., Zhou, G., Tang, Y., Chu, L., Liu, C., Zeng, Z., and Luo, S. New double network hydrogel adsorbent: Highly efficient removal of Cd (II) and Mn (II) ions in aqueous solution. *Chemical Engineering Journal*, 275:179-188, 2015.

[16] Ghorai, S., Sinhamahpatra, A., Sarkar, A., Panda, A. B., and Pal, S. Novel biodegradable nanocomposite based on XG-g-PAM/SiO_2: application of an efficient adsorbent for Pb^{2+} ions from aqueous solution. *Bioresource Technology*, 119:181-190, 2012.

[17] Yu, H. R., Hu, J. Q., Liu, Z., Ju, X. J., Xie, R., Wang, W., and Chu, L. Y. Ion-recognizable hydrogels for efficient removal of cesium ions from aqueous environment. *Journal of Hazardous Materials*, 323:632-640, 2017.

[18] Sahraei, R., Pour, Z. S., and Ghaemy, M. Novel magnetic bio-sorbent hydrogel beads based on modified gum tragacanth/graphene oxide: Removal of heavy metals and dyes from water. *Journal of Cleaner Production*, 142:2973-2984, 2017.

[19] Ho, Y. S. Review of second-order models for adsorption systems. *Journal of Hazardous Materials*, 136(3):681-689, 2006.

[20] d'Halluin, M., Rull-Barrull, J., Bretel, G., Labrugere, C., Le Grognec, E., and Felpin, F. X. Chemically modified cellulose filter paper for heavy metal remediation in water. *ACS Sustainable Chemistry & Engineering*, 5(2):1965 1973, 2017.

[21] Ai, L., Li, M., and Li, L. Adsorption of methylene blue from aqueous solution with activated carbon/cobalt ferrite/alginate composite beads: Kinetics, isotherms, and thermodynamics. *Journal of Chemical and Engineering Data*, 56(8):3475–3483, 2011.

[22] Ai, L., Zhang, C., and Meng, L. Adsorption of methyl orange from aqueous solution on hydrothermal synthesized Mg–Al layered double hydroxide. *Journal of Chemical and Engineering Data*, 56(11):4217–4225, 2011.

[23] Shah, L. A., Khan, M., Javed, R., Sayed, M., Khan, M. S., Khan, A., and Ullah, M. Superabsorbent polymer hydrogels with good thermal and mechanical properties for removal of selected heavy metal ions. *Journal of Cleaner Production*, 201:78-87, 2018.

[24] Song, L., Liu, F., Zhu, C., and Li, A. Facile one-step fabrication of carboxymethyl cellulose based hydrogel for highly efficient removal of Cr (VI) under mild acidic condition. *Chemical Engineering Journal*, 369:641-651, 2019.

[25] Deng, S., Bai, R., and Chen, J. P. Aminated polyacrylonitrile fibers for lead and copper removal. *Langmuir*, 19(12):5058-5064, 2003.

[26] Wang, X., Zhang, B., Zhang, W., Yu, M., Cui, L., Cao, X., and Liu, J. Super-light Cu@ Ni nanowires/graphene oxide composites for significantly enhanced microwave absorption performance. *Scientific Reports*, 7:1–13, 2017.

[27] Burungale, V. V., Devan, R. S., Pawar, S. A., Harale, N. S., Patil, V. L., Rao, V. K., and Patil, P. S. Chemically synthesized PbS nanoparticulate thin films for a rapid NO_2 gas sensor. *Materials Science-Poland*, 34(1):204-211, 2016.